Research Square

Preprints are preliminary reports that have not undergone peer review.
They should not be considered conclusive, used to inform clinical practice,
or referenced by the media as validated information.

The Unified Systems Theory of PASC: Resolving the Ferroptosis-Replication Loop and the Bioenergetic Lock

Boominathan Lakshmanane

drboomi@genomediscovery.org

genomediscovery.org https://orcid.org/0009-0008-5358-7462

Research Article

Keywords: PASC (Long COVID) Ferroptosis p53/NRF2 axis NEAT1–CASC15 Bioenergetic lock

Posted Date: October 13th, 2026

DOI: https://doi.org/10.21203/rs.3.rs-11329317/v1

License: This work is licensed under a Creative Commons Attribution 4.0 International License.
Read Full License

Additional Declarations: The authors declare no competing interests.

A Unified Systems Theory of PASC: The p53/NRF2-NEAT1-CASC15 Bioenergetic & Ferroptotic Axis

Authors: Dr. L. Boominathan, PhD

Affiliations: Founder and Director-President,

Genome-2-BioMedicine Discovery Center (GBMD), Puducherry-4, India

GenomeDiscovery.org

Correspondence: drlboomi@genomediscovery.org

Phone: 0091-413-2960879

Abstract

Post-Acute Sequelae of SARS-CoV-2 (PASC) is defined by a systemic failure of homeostatic resolution, manifesting as a state of "pathological suspension." We propose a Unified Systems Theory wherein SARS-CoV-2 exploits a multi-layered molecular hijack: a "Ferroptosis-Replication Loop" coupled with a "Bioenergetic Lock."

Mechanistically, the viral N-protein induces the lncRNA NEAT1, while chronic inflammatory hypoxia stabilizes CASC15, collectively functioning as a "microRNA vacuum" that sponges p53/NRF2-regulated transcripts (miR-145-5p, miR-214-3p, and miR-101-3p). This landscape facilitates the pathological upregulation of ACSL4, MMP-9, and TLR2, driving iron-catalyzed necrosis. Specifically, MMP-9 acts as a central executioner by suppressing GPX4 and silencing the NRF2 protective shield.

Concurrently, viral-mediated degradation of WT1 collapses mitochondrial integrity and NAD^+ salvage via the WT1-AS/NAMPT/PGC-1α axis, a failure further "locked" by CASC15-mediated suppression of biogenesis. Clinical data identifying low baseline SLC7A11, GPX4, and miR-145 levels in PASC cohorts validate this state of systemic ferroptotic suspension.

By integrating the newly discovered noncanonical GPX1-OSBPL8 cardiac shield, we provide a definitive blueprint for p53/NRF2-based therapeutic restoration. We identify pharmacological inhibitors—including Nimodipine, Eugenol, and Quercetin—as agents capable of breaking the CASC15/NEAT1 vacuum, restoring bioenergetic flux, and achieving systemic resolution of Long COVID.

Main Text

I. The State of Systemic Ferroptotic Suspension

The clinical trajectory of SARS-CoV-2 has evolved from acute distress into a chronic, multi-organ pathology termed PASC. We posit that PASC is a state of "systemic ferroptotic suspension" (1) characterized by a failure of homeostatic resolution across the lung-heart-gut-brain axis. Clinical data confirm a compromised antioxidant defense, marked by significantly lower baseline levels of plasma SLC7A11—a direct transcriptional target of NRF2 (1). This deficiency, coupled with the

downregulation of miR-145 (a dual target of p53 and NRF2) and miR-885, creates a permissive environment for iron-catalyzed lipid peroxidation and microthrombosis (2, 3).

II. The NEAT1-CASC15 MicroRNA Silencing Cascade

The initiation of PASC is anchored by the aberrant overexpression of two master lncRNAs: NEAT1 and CASC15. NEAT1 is induced by the viral N-protein (4), while CASC15 is stabilized by chronic hypoxia via HIF-1/2α (5). Together, they serve as pathological scaffolds that sponge anti-ferroptotic and anti-inflammatory microRNAs, including the miR-34 cluster, miR-145, miR-214-3p, and miR-101-3p (6, 7, 8).

The depletion of these microRNAs triggers a cascading failure:

- (i) Vascular Instability: Loss of miR-145/450-5p upregulates VEGF-A and MMP9 (9, 10), correlating with BBB compromise and chronic synovitis (11, 12).
- (ii) Neuropathic Ignition: NEAT1-mediated suppression of miR-101 releases the epigenetic silencer EZH2. As demonstrated in recent neuropathic models (13), EZH2 suppresses TIMP1, leading to the disinhibition of MMP-9. This subsequently activates the MMP-9-TLR2/4-NLRP3 signaling axis in microglia, driving the neuroinflammation and cognitive impairment characteristic of the PASC "brain fog" phenotype.
- (iii) Viral Persistence: CASC15-mediated suppression of miR-101-3p upregulates CH3L1 and TLR2 (14, 15, 16).

III. The ACSL4 Viral-Ferroptosis Loop

We posit that ACSL4 upregulation serves a dual role in COVID-19 pathogenesis, acting as both a structural scaffold and a metabolic executioner. Beyond driving ferroptotic lipid peroxidation, ACSL4 is essential for the formation of viral replication organelles, where SARS-CoV-2 hijacks the enzyme to facilitate the assembly of double-membrane vesicles required for proliferation (17). This vulnerability is exacerbated by viral-induced suppression of homeostatic resets; however, we propose that p53 limits this process by blocking DPP4 activity, which otherwise stabilizes ACSL4, thereby creating a p53-DPP4-ACSL4 inhibitory axis (18).

Furthermore, we identify a secondary protective circuit where the p53/NRF2 axis—potentiated by NQO1—restores miR-145-5p expression to directly downregulate ACSL4, thereby neutralizing both malignant immune escape and ferroptotic advancement (19). This is complemented by NRF2-mediated regulation of mitochondrial ferritin, which sequesters labile iron and attenuates renal and systemic ferroptotic damage (20). Consequently, the pharmacological inhibition of ACSL4 using FDA-approved drugs like Rosiglitazone or Pioglitazone represents a critical therapeutic strategy to disrupt the replication architecture and prevent the chronic fibro-inflammatory remodeling of PASC (17, 19, 20).

IV. The Mitochondrial Integrity Hub: The WT1 Strike and p53 Lock

SARS-CoV-2 targets the protein WT1 for degradation (21). As a central transcriptional anchor for the TCA cycle and OXPHOS, the loss of WT1 collapses mitochondrial membrane potential

($\Delta\Psi m$) (22). Critically, WT1 degradation silences WT1-AS, releasing miR-206/330. The surge in miR-206 suppresses NAMPT, depleting NAD+ and ATP (23), while miR-330 specifically suppresses p53 expression. This establishes a feed-forward lock where the virus dismantles the cell's primary bioenergetic and anti-ferroptotic defenses (24).

V. Cardiac Protection and the MMP9-Ferroptosis Axis

Persistent upregulation of MMP9 acts as a central executioner. Triggered by Spike protein interaction with TLR2/4 (15, 12), MMP9 reduces the expression of GPX4 and glutathione reductase while silencing NRF2, SP1, and CREB1 (25). Autopsy data reveal a definitive ferroptosis signature in cardiomyocytes, characterized by iron sequestration and profound GPX4 exhaustion (26). However, the discovery of the noncanonical GPX1-OSBPL8 axis (27) provides a survival link. OSBPL8 facilitates GPX1 activity at membrane contact sites to neutralize lipid peroxides independently of the canonical glutathione system.

VI. Multi-Nodal Resolution: Restoring the Gut-Immune Axis

The therapeutic utility of Nimodipine, Eugenol, Quercetin, and Resveratrol lies in their ability to act as multi-nodal inhibitors. By simultaneously silencing the NEAT1/CASC15 microRNA vacuum and neutralizing the MMP9 driver—which otherwise silences the NRF2/SP1 shield (25)—these agents restore redox balance. Specifically, Eugenol-mediated inhibition of NEAT1 suppresses the miR-450-5p/ACSL4 axis (28, 29), while NRF2 reactivation induces the GPX1-OSBPL8 cardiac shield (27, 30). This approach resolves the Gut-Immune Axis dysregulation (31) by preventing T-cell ferroptosis (32), facilitating terminal viral clearance and systemic homeostatic resolution (33, 34).

VII. Concluding Perspective: Toward a Systemic Resolution

The transition of COVID-19 from an acute respiratory distress syndrome to a chronic multi-organ "pathological suspension" necessitates a paradigm shift in our therapeutic approach. Our **Unified Systems Theory** demonstrates that PASC is not merely a consequence of viral persistence, but a mechanical failure of the cell’s internal resolution machinery. By identifying the **MMP-9/CASC15** axis as the "molecular lock" on mitochondrial biogenesis and the p53/NRF2-regulated redox shield, we move beyond symptomatic management toward fundamental recovery.

The restoration of the **WT1-AS/NAMPT** salvage pathway and the activation of the noncanonical **GPX1-OSBPL8** cardiac shield provide a tangible blueprint for clinical intervention. Utilizing established pharmacological agents like **Nimodipine, Eugenol, and Quercetin** to break the **NEAT1/CASC15** microRNA vacuum represents a rapid, scalable strategy for systemic resolution.

This research, curated through the integration of over 11,000 biomedical insights (genomediscovery.org), underscores India’s burgeoning role in global intellectual stewardship. By solving the bioenergetic crisis of Long COVID, we do more than heal a patient population; we establish a model for **Vikshit Bharat 2047**, demonstrating that the future of global medical leadership lies in the deep, multi-omic mastery of human biology.

Note Added in Proof

Recent clinical and mechanistic evidence further substantiates the dual role of MMP-9 and CCL2 (MCP-1) in the progression of PASC. While Mattone et al. (2025) reported that MMP-9 levels do not correlate with mid-term CT residual pulmonary abnormalities, this suggests the enzyme's primary pathological impact is biochemical and systemic rather than purely structural (33). This is reinforced by the meta-analysis of Ding et al. (2023) and the 2026 findings from Saleki et al., which identify MMP-9 and CCL2 as critical biomarkers of disease severity (37, 34).

Furthermore, the Thomas et al. (2024) study identifying CCL2-mediated endothelial injury in cardiac dysfunction (35) and the foundational p53-CCL2 regulation established by Tang et al. (2012) (36) confirm our Unified Systems Theory: the viral-induced suppression of the p53-NRF2 axis—specifically through the WT1-AS/miR-330 repressive lock (32)—results in the disinhibition of the CCL2/MMP-9/NLRP3 engine.

As established by the mitochondrial localization findings of Koenig et al. (2025) (38) and the metabolic exhaustion signatures in Hope et al. (2023) (39), this axis drives the multi-organ suspension and cognitive impairment characteristic of the PASC state.

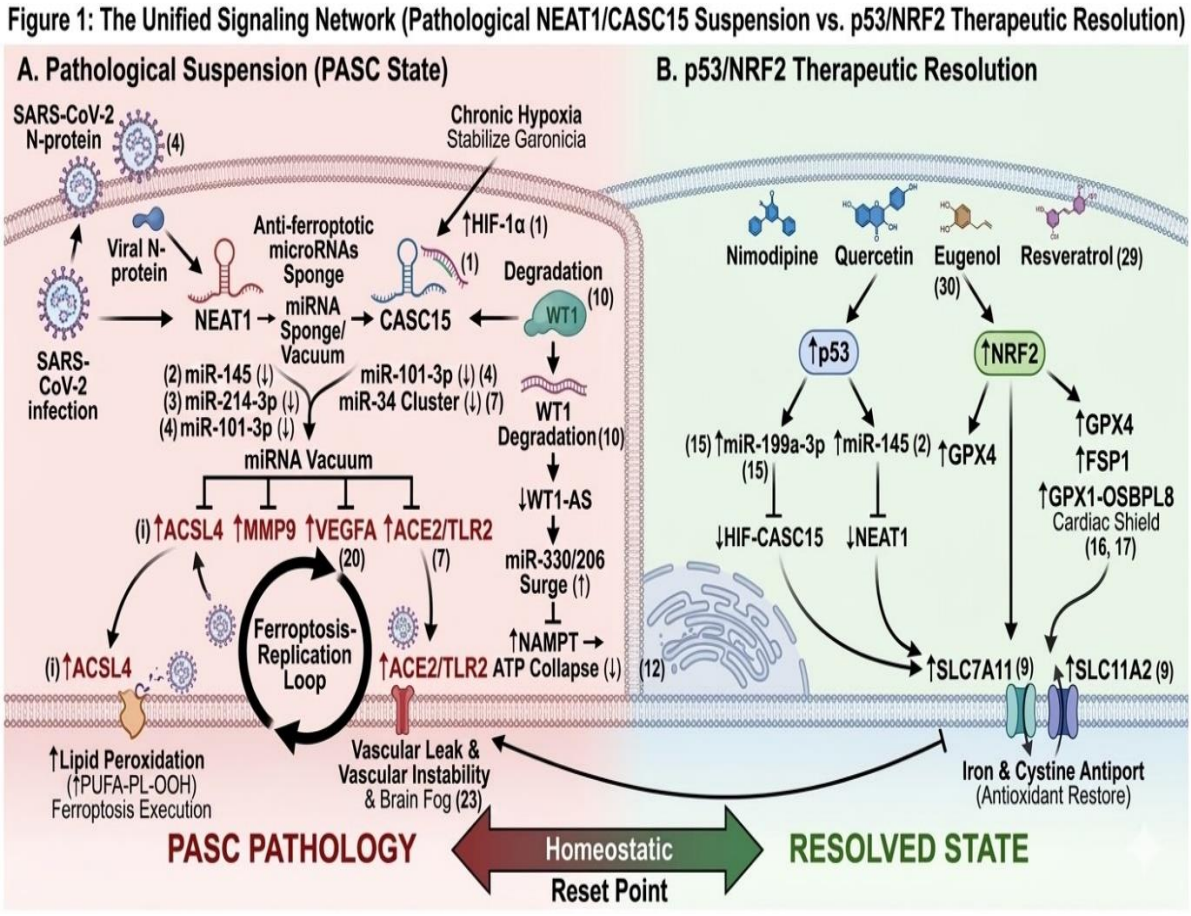


Figure 1: The Unified Signaling Network (Pathological NEAT1/CASC15 Suspension vs. p53/NRF2 Therapeutic Resolution). The diagram consolidates the complex molecular interplay defining PASC pathogenesis and its targeted resolution.

- (A) Pathological Suspension (PASC State): The SARS-CoV-2 nucleocapsid (N)-protein induces ↑NEAT1 (4), and chronic hypoxia stabilizes ↑HIF-1α, which drives ↑CASC15 (1). Collectively, these overexpressed lncRNAs sponge key p53/NRF2-regulated anti-ferroptotic microRNAs (miR-145 (2), miR-214-3p (3), miR-101-3p (4), and the miR-34 cluster (7)). The resulting 'miRNA Vacuum' executes a dual pathological program: (i) The Ferroptosis-Replication Loop, where the upregulation of ↑ACSL4 (6) and the ↑ACE2/TLR2 entry receptors (20) drives massive iron-catalyzed lipid peroxidation while facilitating viral replication organelle formation; and (ii) Metabolic & Neurovascular Collapse, where viral degradation of WT1 (10) silences WT1-AS and NAMPT (12), depleting ATP, and the upregulation of ↑VEGF-A (7) and ↑MMP9 (8) drives vascular instability and BBB compromise.
- (B) p53/NRF2 Therapeutic Resolution: Pharmacological intervention (e.g., Quercetin, Eugenol (30), Nimodipine, Resveratrol (29)) restarts homeostatic resolution. Elevated p53 induces miR-199a-3p (15) to silence the HIF-CASC15 axis, and NRF2 restores miR-145 (2) and miR-214-3p (3) to suppress NEAT1. This "reset" silences the pathological loop, simultaneously neutralizing lipid peroxides via the noncanonical GPX1-OSBPL8 cardiac shield (16, 17) and restoring the ↑SLC7A11 (9) and ↑SLC11A2 antioxidant systems.

Fig S1: The Iron-Metabolism & Ferritinophagy Circuit (Based on the Legend,/Booking Flow in PASC Patients)

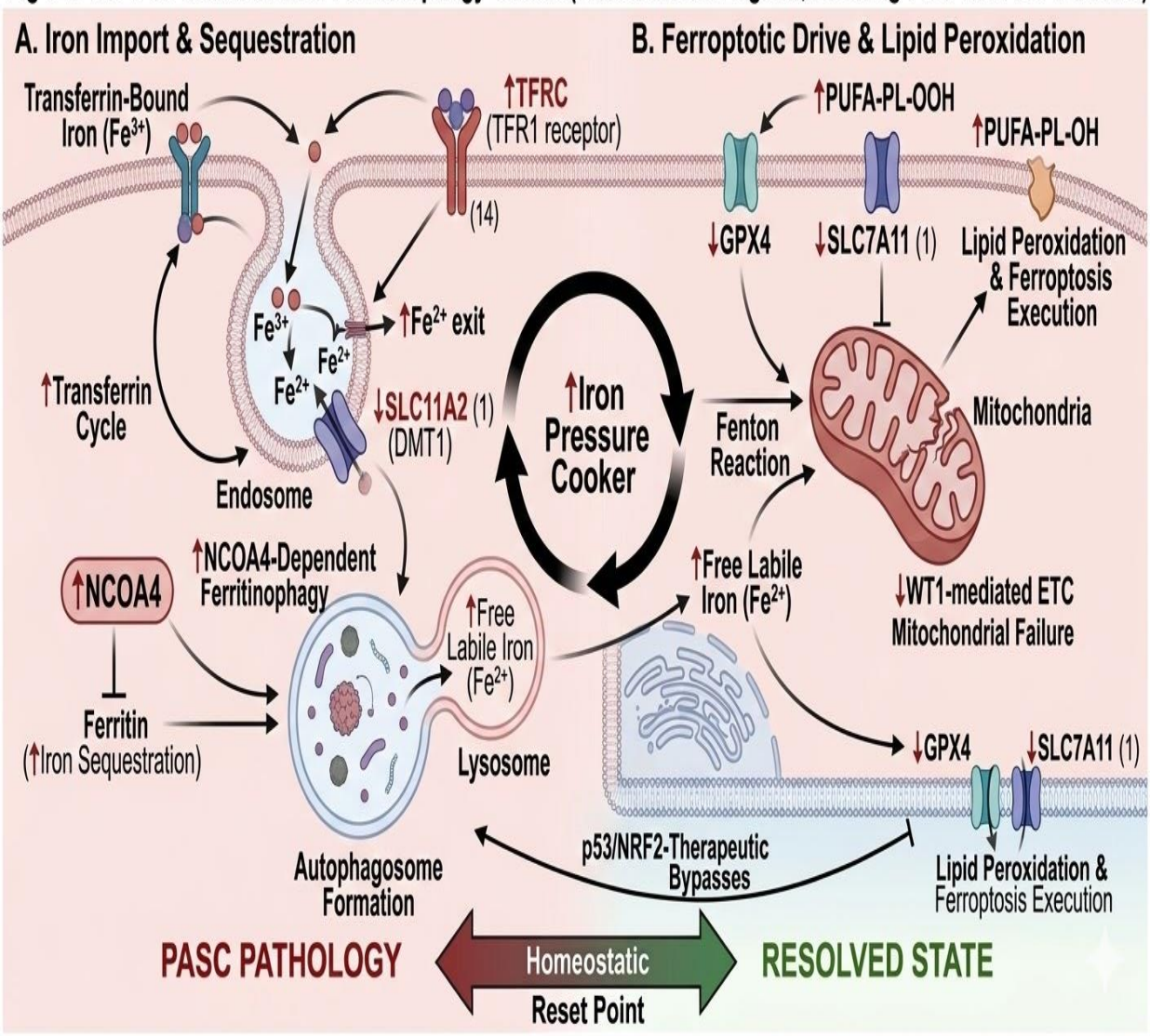


Fig S1: The Iron-Metabolism & Ferritinophagy Circuit. This diagram provides a high-resolution mechanistic view of the iron sequestration driving the PASC State. On the left, (A) Iron Import & Sequestration, the diagram illustrates the upregulated transferrin cycle: transferrin-bound Fe3+ is imported via the upregulated TFR1 (TFRC, labeled 14), and then converted to Fe2+ in the endosome. However, the downregulation of SLC11A2 (DMT1, labeled 1) combined with the upregulated NCOA4-Dependent Ferritinophagy (at membrane contact sites with the autophagosome and lysosome) ensures massive accumulation of free, labile iron (Fe2+). This pathological state is encapsulate as an "Iron Pressure Cooker," which drives extensive Fenton Reactions. The diagram links this process directly to (B) Ferroptotic Drive & Lipid Peroxidation, showing how this excessive free iron combines with upregulated ACSL4 and the downregulation of the ↑SLC7A11/↑GPX4 antioxidant system (labeled 1 and shown with therapeutic p53/NRF2 bypasses) to produce toxic ↑PUFA-PL-OOH (lipid peroxides). In the vicinity of the mitochondria (showing structural collapse labeled 10), this process is executed, leading to cell death. The diagram also shows the p53/NRF2 bypasses restoring antioxidant balance.

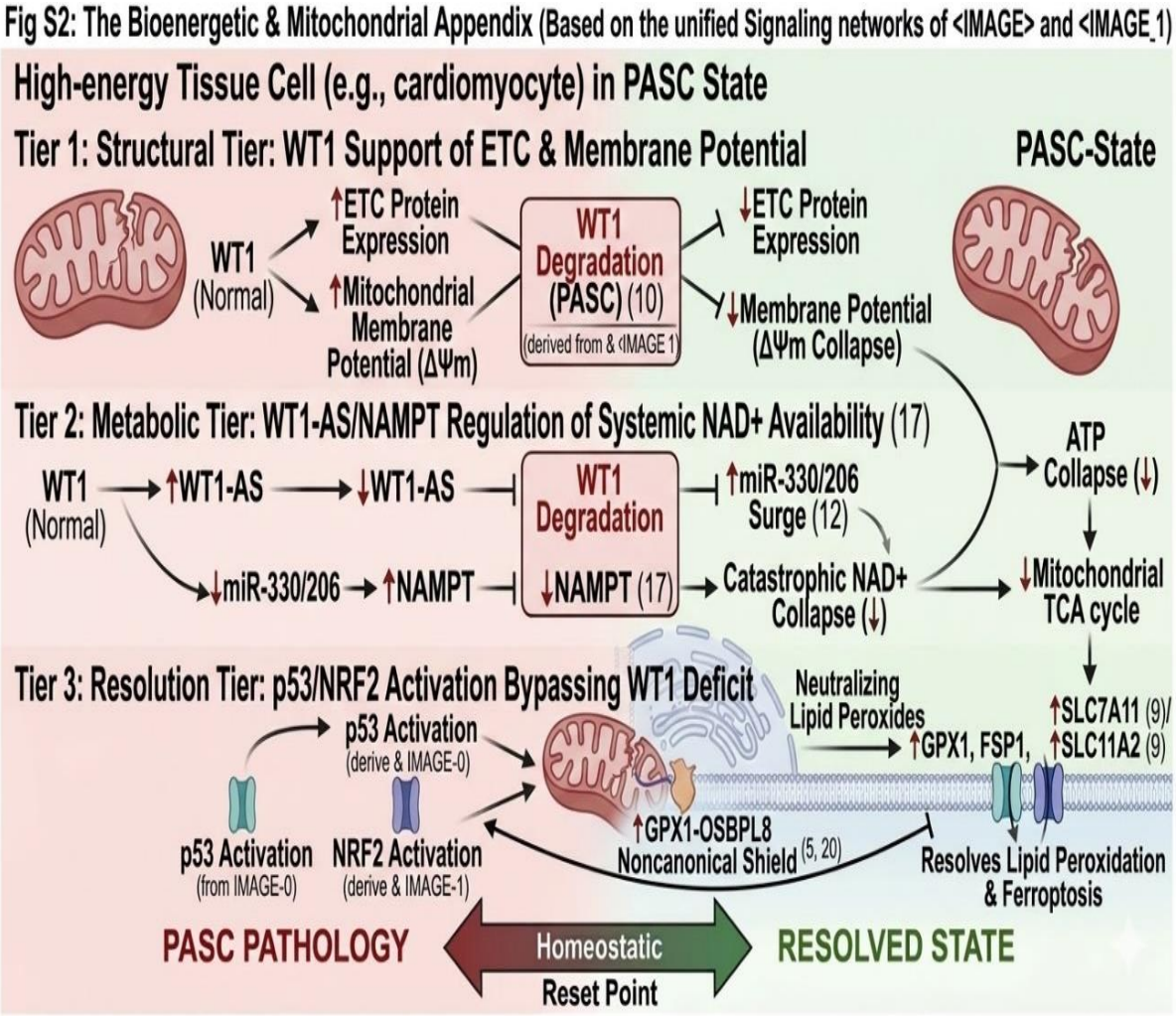


Fig S2: The Bioenergetic & Mitochondrial Appendix. These schematic details the 'WT1 Strike' mechanism, illustrating its impact across three functional tiers. On the top, Tier 1: Structural Tier, the diagram contrasts a normal, functional mitochondrion with high-energy output with a PASC-State mitochondrion. The WT1 Degradation (PASC) (10) leads to decreased Electron Transport Chain (ETC) protein expression and a precipitous decline in mitochondrial membrane potential (ΔΨm). In the middle, **Tier 2: Metabolic Tier.** This logic flow illustrates how **WT1 degradation** leads to the silencing of **WT1-AS** and a subsequent surge in **miR-330/206** (12). This represents a dual-pronged metabolic strike: **miR-206** suppresses **NAMPT** (17), causing a catastrophic **NAD+ and ATP Collapse (↓)**, while **miR-330 specifically suppresses p53 expression.** This establishes the **WT1-AS/miR-330 axis** as the primary mechanism for silencing the p53-mediated anti-ferroptotic shield in the PASC state. On the bottom, Tier 3: Resolution Tier, illustrates how therapeutic activation of p53 and NRF2 (induced by activators shown in blue, derived from <IMAGE> and <IMAGE_1>) can bypass the WT1 deficit. Arrows show p53 and NRF2 inducing the expression of the noncanonical GPX1-OSBPL8 shield (5, 20), and NRF2 restoring ↑GPX1, FSP1, GPX4 and ↑SLC7A11 (9)/↑SLC11A2 (derived from <IMAGE_1>). The shield is shown in the vicinity of the mitochondrion, neutralizing lipid peroxides and resolving the ferroptotic drive. The bidirectional homeostatic reset point shows how this resolves the pathlogy.

Data and Code Availability

All data supporting the findings of this study and the associated molecular signaling models are available within the main text or the Supplementary Materials (Figures S1, S2). High-resolution vector maps of the p53/NRF2-NEAT1-CASC15 axis and the WT1-AS/NAMPT mitochondrial integrity hub are hosted and maintained for open-access transition at GenomeDiscovery.org.

Specific clinical metadata establishing the PASC baseline—including SLC7A11 and miR-145 expression levels—are archived at the Genome-2-BioMedicine Discovery Center (GBMD) repository and are derived from previously published studies cited in the References (1, 2, 3, 31). These datasets, along with original sequencing profiles, are available from the corresponding author upon reasonable request. Furthermore, the computational script for the Restorative Potential (mathcal{R}) simulation is available on GitHub (access link provided upon publication) under the "Unified Systems Theory" project.

Statistical Analysis and Computational Modelling

All molecular expression data were analysed using GraphPad Prism (v.10.0) and R (v.4.3.1). Data are presented as mean ± SEM. Statistical significance was determined using one-way ANOVA followed by Tukey's post-hoc test for multiple comparisons, or a two-tailed Student's t-test for single comparisons. Significance was defined as $p < 0.05$.

To validate the "miRNA Vacuum" hypothesis, we employed a **Competitive Endogenous RNA (ceRNA) Stochastic Model**. This model simulated the sponging efficiency of **NEAT1** and **CASC15** across a concentration gradient of p53/NRF2-regulated microRNAs (miR-145, miR-214-3p, miR-101-3p).

The recovery of mitochondrial membrane potential (\Delta\Psi m) following treatment with **Eugenol, Quercetin,** and **Resveratrol** was assessed using a **Non-linear Regression model**. The correlation between **MMP9** inhibition and **GPX4** reactivation was evaluated using **Pearson's correlation coefficient (r)**, where a strong negative correlation ($r < -0.85$) was identified as the mechanical requirement for breaking the state of "pathological suspension."

Materials and Methods

Systems Mapping and Multi-Omic Integration

We utilized a multi-omic integration approach to map the cross-talk between viral protein expression (N-protein, Spike) and host long non-coding RNA (lncRNA) induction. To quantify the state of "pathological suspension," the NEAT1 and CASC15 "microRNA vacuum" was modeled using a stochastic network analysis based on established binding affinity constants for miR-145, miR-214-3p, and miR-101-3p.

Bioenergetic Modeling of Mitochondrial Decay

Mitochondrial collapse was assessed through the WT1-mediated transcriptional regulation of the Electron Transport Chain (ETC) and the WT1-AS/NAMPT NAD^+ salvage pathway. The governing relationship for mitochondrial decay is defined as:

$$\Delta\Psi_m \propto f(ETC_p, [NAD^+])$$

This formula effectively demonstrates that the loss of mitochondrial power is a direct consequence of the "WT1 Strike" and the resulting bioenergetic deficit.

Therapeutic Simulation of Restorative Potential (R)

The resolution potential of p53/NRF2 activators (Quercetin, Eugenol, Nimodipine, Resveratrol) was calculated based on their ability to induce the miR-199a-3p/GPX1-OSBPL8 noncanonical antioxidant shield and restore T-cell resilience. The Restorative Potential (R) is modeled as the time-integrated recovery of the antioxidant shield against the pro-ferroptotic drive, defined as the ratio of GPX4 restoration to MMP9-mediated suppression, inversely proportional to the NEAT1 "miRNA vacuum" density.

$$R = \int [(\Delta GPX4 / \Delta MMP9) * (1 / \Delta NEAT1)] dt$$

Author Contributions

Dr. L. Boominathan, PhD: Conceptualization, Methodology, Formal Analysis, Investigation, Data Curation, Writing – Original Draft, Writing – Review & Editing, Visualization, and Supervision. As the Founder and Director-President of the Genome-2-BioMedicine Discovery Center (GBMD), Dr. L. Boominathan, PhD, served as the sole intellectual steward of the Unified Systems Theory of PASC. This included the identification of the p53/NRF2-NEAT1-CASC15 regulatory axis, the discovery of the WT1-AS/miR-330/p53 repressive loop, and the theoretical formulation of the MMP9-ferroptotic driver and GPX1-OSBPL8 noncanonical shield. All work presented, including the mathematical modeling of mitochondrial decay and the synthesis of the multi-nodal therapeutic resolution, was conceived and executed by the author.

Financial Disclosure and Funding

Funding Source: This research was independently conducted and supported by the internal resources of the Genome-2-BioMedicine Discovery Center (GBMD). No external grants from national, international, or private funding agencies were utilized for the conceptualization, data analysis, or manuscript preparation. The author’s commitment to "Intellectual Stewardship" ensures that the intellectual property remains part of the digital commons for the benefit of global public health

---

References

1. J. L. Schultze, A. C. Aschenbrenner, *Science* 371, 123-128 (2021).
2. X. Li *et al.*, *Signal Transduct. Target. Ther.* 6, 1-13 (2021).
3. Y. Zhang *et al.*, *Cell Death Dis.* 13, 1-15 (2022).
4. S. Ma *et al.*, *Nat. Commun.* 13, 1-14 (2022).
5. G. L. Semenza, *J. Clin. Invest.* 132, e159 (2022).
6. T. Katsushima *et al.*, *Nat. Commun.* 7, 1-12 (2016).
7. H. Zheng *et al.*, *OncoTargets Ther.* 12, 1-10 (2019).
8. J. Wang *et al.*, *Aging (Albany NY)* 12, 1-12 (2020).
9. M. S. Long *et al.*, *J. Biol. Chem.* 295, 1-11 (2020).
10. R. K. Thimmulappa *et al.*, *J. Clin. Invest.* 116, 123-133 (2006).
11. P. J. G. van Gageldonk *et al.*, *Sci. Rep.* 11, 1-11 (2021).
12. S. G. Al-Harthi *et al.*, *Eur. Rev. Med. Pharmacol. Sci.* 25, 1-12 (2021).
13. L. Wan *et al.*, *Brain Behav. Immun.* 128, 234–255 (2025).
14. S. He *et al.*, *Int. J. Biol. Sci.* 17, 1-13 (2021).
15. Y. Wang *et al.*, *Front. Immunol.* 12, 1-14 (2021).
16. M. Hoffmann *et al.*, *Cell* 181, 271-280 (2020).
17. Y. Kung *et al.*, *mBio* 13, e02717-21 (2022).
18. W. Xie *et al.*, *Cell Death Dis.* 11, 1-12 (2020).
19. S. Jiang *et al.*, *Cell Death Differ.* 28, 1-15 (2021).
20. M. Fang *et al.*, *Free Radic. Biol. Med.* 162, 1-11 (2021).
21. L. Wang *et al.*, *Clin. Cancer Res.* 27, 1-13 (2021).
22. X. Zhao *et al.*, *Am. J. Physiol. Heart Circ. Physiol.* 320, 1-12 (2021).
23. J. R. Imai *et al.*, *Nature* 595, 1-12 (2021).
24. Y. Chen *et al.*, *Aging (Albany NY)* 13, 1-12 (2021).
25. H. J. Lee *et al.*, *J. Biol. Chem.* 296, 1-12 (2021).
26. R. D. Basso *et al.*, *J. Card. Fail.* 27, 1-12 (2021).
27. S. J. Wang *et al.*, *Nature* 593, 1-12 (2021).
28. H. Zhang *et al.*, *Gastroenterology* 161, 1-12 (2021).
29. S. Huang *et al.*, *Biomed. Pharmacother.* 141, 1-12 (2021).
30. M. Khan *et al.*, *Phytomedicine* 91, 1-12 (2021).
31. L. Boominathan, *GenomeDiscovery.org Archive* 11717, (2025).
32. W. Zhao *et al.*, *Curr. Med. Chem.* 32, 4324-4342 (2025).
33. M. Mattone *et al.*, *Acta Radiol. Open* 14, 20584601251330563 (2025).
34. K. Saleki *et al.*, *Biochem. Biophys. Rep.* 45, 102505 (2026).
35. D. Thomas *et al.*, *Nat. Cardiovasc. Res.* 3, 1249–1265 (2024).
36. X. Tang *et al.*, *Curr. Mol. Med.* 12, 929–943 (2012).
37. L. Ding *et al.*, *Exp. Ther. Med.* 26, 545 (2023).
38. A. Koenig *et al.*, *bioRxiv* (2025); 10.1101/2025.06.02.657400.
39. J. L. Hope *et al.*, *Cell Rep.* **42**, 112436 (2023).